# FINITE-DIFFERENCE SIMULATION OF A MULTI-PASS PIPE WELD*

K. K. WAHI, D. E. MAXWELL, J. E. REAUGH

*Science Applications, Incorporated,*
*8201 Capwell Drive, Oakland, California 94621, U.S.A.*

## SUMMARY

An analytical technique to study the thermomechanical response of pipes during welding and subsequent to welding is presented. The numerical simulation was performed using STEALTH, a two-dimensional explicit-finite difference code. A finite difference grid was designed to represent the weld region and a portion of a long, 4-in. diameter butt-welded pipe.

The thermal and temperature-dependent mechanical properties of Type 304 stainless steel were used for both the pipe and the weldment materials. The welding area was subdivided into seven regions. The model for spatial and temporal heat deposition was compatible with the welding speed and conditions reported in relevant G.E. Reports.

Since creep is not included, the residual stresses after cooling depend only on the stress-strain path and not on the total time involved. Therefore, the excess heat in the grid at late times could be withdrawn artificially. This was done by a prescription that smoothly reduced the temperature gradients to achieve ambient conditions. Because the thermal and mechanical responses were computed simultaneously, it was desirable to reduce the disparity between the associated thermal time step and the mechanical time step (based on sound speed). This was achieved by increasing the mechanical time step by employing a density scaling factor of $7.58 \times 10^{11}$ to make the two time steps similar. A dynamic relaxation technique was then used to damp the non-physical mechanical oscillations that were generated by the thermal expansions and contractions.

The comparison of the numerical temperature results with the experimental thermocouple data was not very satisfactory. However, temperature results of a similar calculation performed by using a finite-element approach were in excellent agreement with the finite-difference results. The experimental residual stress results showed large circumferential variation of stress, a feature that could not be simulated in the two-dimensional axisymmetric geometry that was employed. The objectives were (a) to assess the finite-difference computational techniques as applied to this problem and (b) to gain information of mechanisms and processes involved. It is clear that the finite-difference technique is very relevant in solving the dynamic thermo-mechanical problems and has very few limitations. The latter objective was realized in a variety of ways that impact on the application of the numerical codes to the butt welding problem. Some of these are:

1. The importance of realistic thermal boundary conditions to provide the propper cooling temperature gradients.
2. The importance of choosing an appropriate grid length to isolate the end effects from the weldment.
3. The relative non-importance of "coupling" by including the thermal part of the internal energy in the definition of temperature.
4. The importance of interpass annealing between successive passes of the arc.
5. The possibility of employing mechanical annealing procedures to augment post-welding treatment.

* Work performed under the auspices of the Electric Power Research Institute.

## 1. Introduction

The process of welding involves a large excursion of temperatures (including a phase change) and, consequently, a complex pattern of temperature histories. A complex pattern of thermomechanically generated stresses is attendant, and a residual stress field exists at the end of the process. In order to understand the relationship of the residual stresses to the parameters of the welding sequence, it is desirable to have a numerical method of simulating the process. Consequently, it is necessary to develop analytical techniques (or refine the existing ones) to supplement the experimental techniques and measurements. An explicit finite-difference approach was used to perform a large-scale calculation simulating the butt welding of a 4-inch steel pipe. All seven passes were computed, and thermal cooling and stress relaxation between each pass was also allowed. The two-dimensional finite-difference code, STEALTH 2D [4] was used.

## 2. Finite-Difference Formulation and Modeling

### 2.1 Material Models

The thermal and mechanical properties of Type 304 stainless steel were used for both the pipe and the weldment materials. The temperature-dependent material properties at high temperatures had to be extrapolated from data for Type 304 steel at lower temperatures [5]. The derivation of a general thermomechanical model and the relevant input data for material properties may be found in [1].

### 2.2 Bead Deposition Model

The welding area was subdivided into seven regions corresponding to the beads that are deposited at the start of each welding pass. The diagrams of Figure 1 display the sequential deposition of the bead mass at the start of each pass and the associated melt regions outlined by solid dots. The cells shown in each bead are the finite-difference zones for that bead area.

### 2.3 Energy Input Modeling

The model for spatial and temporal heat deposition is compatible with the welding speed and conditions reported in [2]. A uniform spatial heat deposition was specified in each bead region with a rate dependency given by eq. (1).

$$\dot{q}(t) = \eta \dot{q}_o \exp\left[-0.5\left(\frac{t}{\tau} - 3\right)\right] \qquad (1)$$

where

$\dot{q}$ is the instantaneous rate ($W/m^3$),

$\eta$ is the efficiency ($< 1$), to account for electrode losses,

$\dot{q}_o$ is the peak rate, normalized by conservation of energy,

$\tau$ is the characteristic time, based on the time required for the bead to travel one electrode diameter.

The time, t, is normalized to zero at the start of each pass. The values of the various parameters of eq. (1) are given in Table 1.

### 2.4 Boundary Conditions

Due to economic constraints, only a short section of the pipe was considered. Traction-free conditions were prescribed on all boundaries. However, a shear distortion constraint was imposed on the two ends to eliminate bending in order to provide a better approximation

of the true strain condition at that position for the long pipe.

The complete computational grid, including the thermal and mechanical boundary conditions, is shown in Figure 2. The outer boundaries in the weldment region vary according to the pass number. Positions 1, 2, and 3 in Figure 2 correspond to thermocouple locations. Radiation and convection losses are allowed to occur on the inner and outer surfaces of the pipe. These losses were modeled as

$$\dot{E}_{rad}(W/m^2) = 0.6\sigma(T^4 - T_o^4) \tag{2}$$

$$\dot{E}_{conv}(W/m^2) = 5.886(T - T_o) \tag{3}$$

where $\sigma$ is the Stephen-Boltzmann constant and the factor of 0.6 corresponds to a reasonable average emissivity [6]. The convective coefficient 5.886 is a reasonable value for cooling in static air. The top and bottom (inner and outer) surfaces were adiabatic with respect to heat conduction, whereas isothermal (ambient temperature) conditions were prescribed at the left and right boundaries. Clearly, the proper end condition is somewhere between isothermal and adiabatic to account for the real heat conduction at this location in the long physical pipe.

### 2.5 Late-Time energy Loss Modeling

Since creep is not included in this simulation, the residual stresses after cooling depend only on the stress-strain path and not on the total time involved. After about 30 seconds, following the start of each pass, the grid was cooling essentially everywhere. Therefore, the excess heat was withdrawn from the grid after this time by a prescription that smoothly decreased the gradients to achieve ambient temperature.

### 2.6 Density Scaling and Dynamic Relaxation

Because the thermal and mechanical responses were computed simultaneously, it was desirable to reduce the disparity between the associated thermal time step and the mechanical time step (based on sound speed). This was achieved by increasing the mechanical time step by employing a density scaling factor of $7.58 \times 10^{11}$ to make the two time steps similar. An example of the density scaling technique may be found in [3]. A dynamic relaxation technique was then used to damp the non-physical mechanical oscillations that were generated by the thermal expansions and contractions. The damping frequencies were a function of the energy deposition time during the heating phase, and of the sound speed transit times through the pipe wall thickness ($\approx$ 1.5 seconds) and along its half-length ($\sim$ 6 seconds) during cooling. These transit times are based on the scaled density. Such a large density scaling was possible because momentum effects in this case are trivial.

## 3. Temperature Results and Comparisons

### 3.1 Melt Regions

The maximum region of melt for each pass was defined by the condition that the solidus temperature was reached at some time inside the region. The melt regions for the seven passes are outlined in Figure 1 by solid dots. The largest displacements occurred during energy deposition and appeared in the melted region, and were a significant fraction of a zone width.

### 3.2 Temperature Response

Pass 1 temperatures versus time are displayed in Figure 5 at selected points on the

inner surface of the pipe and compared to the corresponding thermocoupld data [2]. The experimental response was limited to the range of 399°C to 1093°C (750°F to 2000°F) and the time origin was arbitrary. The differences are large and are probably due to a variety of reasons:

1. Property model assumptions.
2. Energy deposition model assumptions.
3. 2D simulation of 3D experiment.
4. Non-ideal experimental features:
   thermocouple response errors;
   interruptions during a welding pass.

An examination of the thermocouple data for other passes shows:

(a) frequent thermocouple response anomalies, similar to thermocouple 3 of Figure 5;

(b) generally slower rising and falling temperature histories compared to the computed results, similar to thermocouple 2 of Figure 5;

(c) peak temperatures were erratic compared to the computed data.

Experimental interpass temperatures were not recorded, but were noted to be less than 177°C (350°F) for Passes 4 through 7 [2]. There may be a significant error in the calculations which assumed ambient temperature (20°C) between all passes.

Pass 1 inner surface temperatures versus distance from the centerline are shown in Figure 6 at selected times for this calculation. In the temperature contours of Figure 3, it can be seen that the isotherms intersect the inner and outer surfaces at essentially right angles. This would not be true if the heat flux associated with surface losses were comparable to the longitudinal flux due to conduction to the isothermal end condition. Thus, an adiabatic condition on the ends of the grid must produce a different cooling and straining pattern at late times and may lead to quite different residual stresses.

### 3.3 Thermal Boundary Condition Effects

The isothermal boundary condition applied at the ends of the pipe in this calculation produced late-time cooling gradients that were oriented along the length of the pipe. In contrast, adiabatic end conditions must produce radially oriented gradients. Thus, the adiabatic and isothermal end conditions led to different late-time cooling temperature gradients that correspond, respectively, to the "through-wall" and "non-through-wall" temperature gradient cases discussed in [2]. For isothermal end conditions, residual stresses should be substantially lower than for adiabatic end conditions.

### 3.4 Pipe Length Effects

The time-dependent plastic region in the calculation approached the ends of the finite-difference grid. The residual strains were large in the plastic regions and small near the ends in the elastic regions. The final displacements indicated that wall thickness at the two ends is essentially unchanged after seven passes. Ideally, the grid should be long enough so that a large elastic region would isolate the weldment from the ends to simulate a long pipe case. This was not true in this calculation.

### 3.5 Interpass Stress Annealing Effects

In order to limit the computer costs, the calculations were speeded up by (a) enhancing the late-time cooling rate in a prescribed manner and (b) by not achieving true stress-strain equilibrium for the intermediate passes. The former approximation is justified since

the plastic domain is shrinking before the enhanced cooling is applied and the temperature gradients do not change direction as they diminish during late-time cooling. The latter would be justified if the interpass residual stresses were effectively annealed by the heat of the subsequent passes. A qualitative demonstration of the annealing effect was observed. The pressure history of a cell far removed from the bead regions was monitored for Passes 4, 5, 6, and 7. It was noted that the pressure responses were similar for Passes 4 and 6, and the bead centers were located at approximately the same distance from the cell being monitored [1]. Likewise, Passes 5 and 7 had similar pressure responses and were similarly located. It is concluded that the interpass stresses are effectively annealed by the subsequent pass heating and that Pass 7 dominates the final residual stresses.

3.6 Residual Stresses for Pass 7

An examination of the stresses at late times showed that the hoop stress, $T_{\theta\theta}$, and the longitudinal stress, $T_{\ell\ell}$, were much larger than the radial stress, $T_{RR}$, the shear stress, $T_{R\ell}$, and the pressure. Time history plots of various zones showed that $T_{\theta\theta}$ and $T_{\ell\ell}$ were approaching asymptotic values that were only about 10% different from the values reached at the final time of 85 seconds (after the start of Pass 7). Therefore, it was decided to terminate the calculation at this time.

Contours of $T_{\theta\theta}$ and $T_{\ell\ell}$ at the final time are displayed in Figure 4. It can be noted that the stresses at the ends are not well isolated from the weldment region. This indicates that the grid was too short to simulate a long pipe case.

Perhaps the most dominant feature of the experimental residual stress was the large circumferential variation that was observed. This was probably due to the interruptions in the bead deposition. In any case, these variations cannot be modeled by the axisymmetric code geometry and only circumferential averages can be compared.

## 4. Summary and Conclusions

The comparison between the finite-difference temperature results and the experimental thermocouple data mas moderately satisfactory. Some of the differences were undoubtedly due to inaccuracies in the material modeling, interpass ambient temperature assumption, and in the experimental instrumentation. Also, there were differences due to the fact that the calculations corresponded to instantaneous bead deposition in the circumferential direction in contrast to the experimental case with its interrupted and finite welding speed.

One of the more dominant features of the experimental residual stress results was large circumferential variation of stress, a feature that could not be simulated in the two-dimensional axisymmetric geometry that was employed. It was not expected that the analytical stress results could be compared simply with the experimental data. The objectives were (a) to assess the feasibility of using this computational technique to simulate a welding process, and (b) to gain information of mechanisms and processes to aid in the understanding and modeling of the physical case. The former objective was achieved, and the differences between the experiment and calculation are understood. The latter objective was realized in a variety of ways that impact on the application of the numerical technique to the butt welding problem. Some of these are:

1. The importance of realistic thermal boundary conditions to provide the proper cooling temperature gradients.

2. The importance of choosing an appropriate grid length to isolate the end effects from the weldment.
3. The relative non-importance of "coupling" by including the thermal part of the internal energy in the definition of temperature.
4. The importance of interpass annealing between successive passes of the arc.

Although the grid design and modeling procedures were not optimum, this calculation provides a reasonable bench mark for future application of finite-difference codes for thermomechanical problems, such as welding. The computer costs are directly proportional to the product of the number of mesh points and the computational cycles. The pertinent data for this calculation are:

number of grid points = 385

number of computational cycles = 9450

number of zone cycles = 385 X 9450 = 3,638,250

number of CDC 7600 computing hours = 1.82

number of CP hours per million zone cycles = 0.498

## References

[1] Maxwell, D., Wahi, K., "Numerical Analysis of Welds," Final Report prepared for EPRI, Palo Alto, California, Research Project 602-2 (to be published).

[2] Klepfer, H. H., et al., "Investigation of Cause of Cracking in Austenitic Stainless Steel Piping," Vols. 1 and 2, NEDO-21000-1 and -2, 75NED35, General Electric Company, July 1973.

[3] Reaugh, John E., "Calculation of Quasi-Static Elastic-Plastic Deformation with Heat Conduction," American Nuclear Society Transactions, TANSAO 18 1-401 (1974), Vol. 18, June 1974, Philadelphia, Pennsylvania, p. 135.

[4] Hofmann, Ronald, "STEALTH, A Lagrange Explicit Finite-Difference Code for Solids, Structural, and Thermohydraulic Analysis," EPRI NP-176, Electric Power Research Institute, Palo Alto, California, June 1976.

[5] Datsko, J., Material Properties and Manufacturing Processes, John Wiley & Sons, New York, 1966.

[6] Nuclear Systems Materials Handbook, Volume 1, Design Data.

TABLE I. ENERGY INPUT MODEL PARAMETERS

| Welding pass | Bead radius (m) | Bead volume ($m^3$) | $\dot{q}_o$ ($W/m^3$) | $\tau$ (sec) | $\eta$ (%) |
|---|---|---|---|---|---|
| 1 | 0.0512 | $3.604 \times 10^{-6}$ | $3.880 \times 10^{10}$ | 1.125 | 50 |
| 2,3 | 0.0531 | $3.331 \times 10^{-6}$ | $3.726 \times 10^{10}$ | 1.7578 | 40 |
| 4,5 | 0.0552 | $3.543 \times 10^{-6}$ | $7.183 \times 10^{10}$ | 0.4688 | 50 |
| 6,7 | 0.0570 | $4.349 \times 10^{-6}$ | $6.036 \times 10^{10}$ | 0.4688 | 50 |

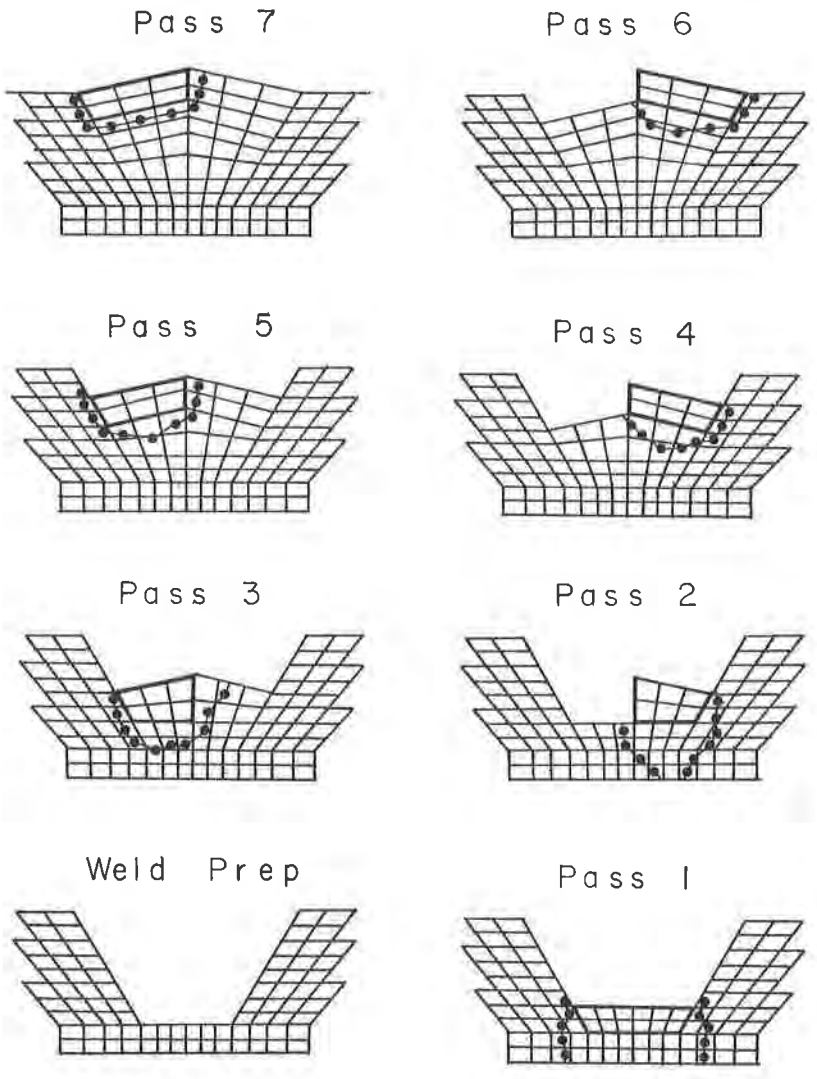


Figure 1 The weld prep section and the regions of maximum melt surrounding each bead.

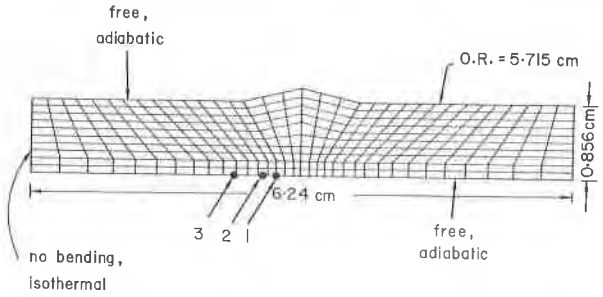


Figure 2 The computational grid and thermomechanical boundary conditions.

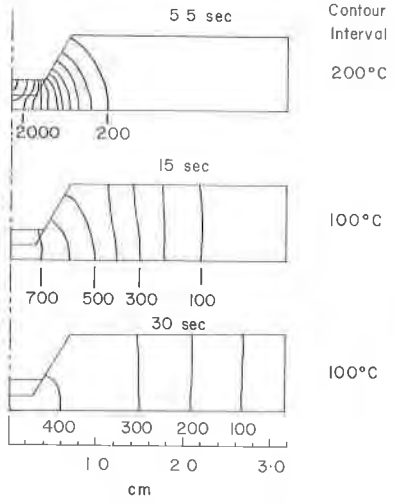


Figure 3 Temperature contours at selected times for Pass 1.

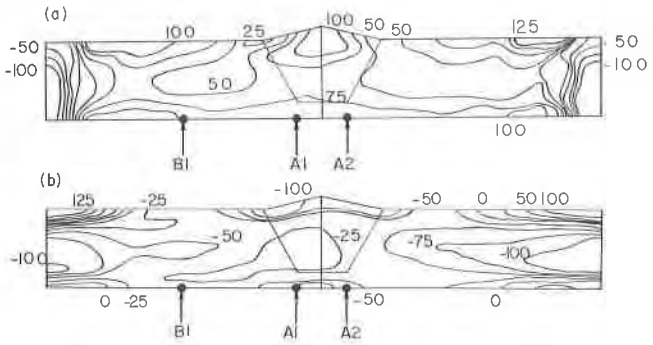


Figure 4 Stress contours at the end of Pass 7.

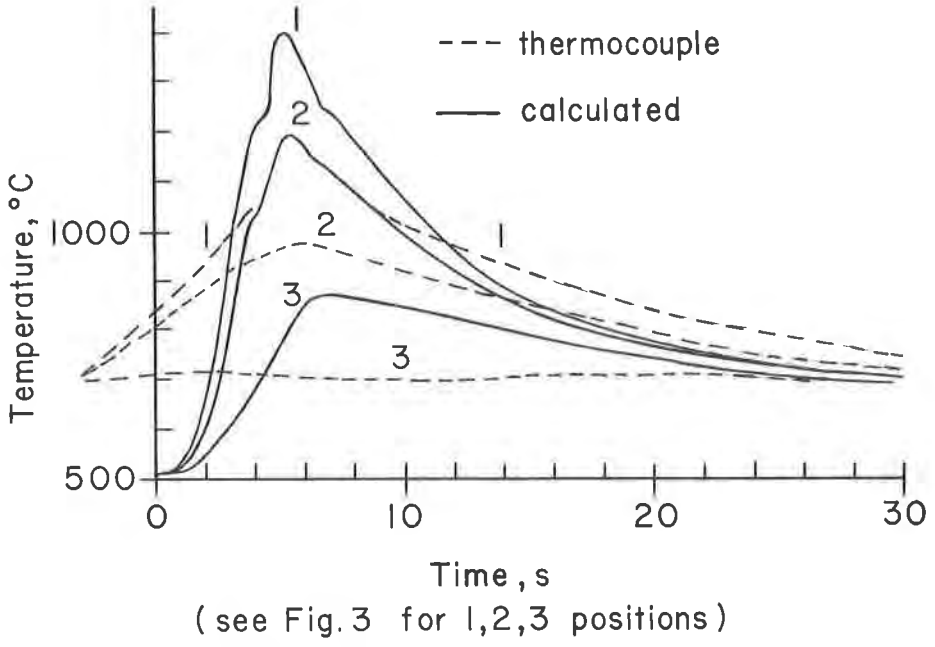


Figure 5 Temperature versus time for Pass 1.

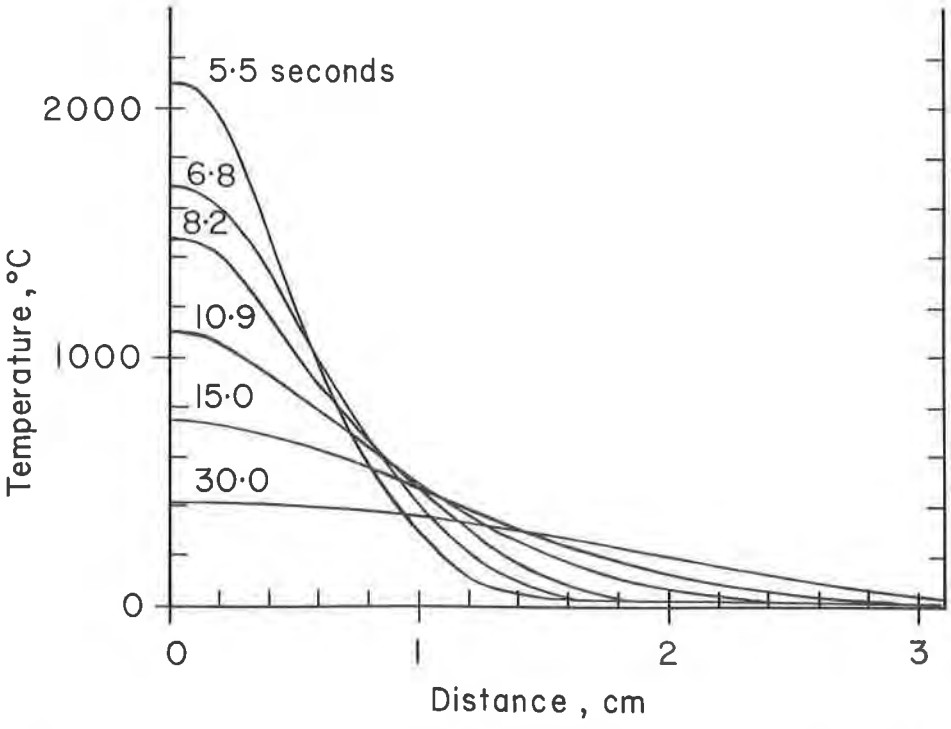


Figure 6 Temperature versus distance from centerline on the inner surface, Pass 1.